

Dust in the wind: Crystalline silicates, corundum and periclase in PG 2112+059

F. Markwick-Kemper,^{1,2} S. C. Gallagher,³ D. C. Hines⁴ & J. Bouwman⁵

ABSTRACT

We have determined the mineralogical composition of dust in the Broad Absorption Line (BAL) quasar PG 2112+059 using mid-infrared spectroscopy obtained with the *Spitzer Space Telescope*. From spectral fitting of the solid state features, we find evidence for Mg-rich amorphous silicates with olivine stoichiometry, as well as the first detection of corundum (Al_2O_3) and periclase (MgO) in quasars. This mixed composition provides the first direct evidence for a clumpy density structure of the grain forming region. The silicates in total encompass $(56.5 \pm 1.4)\%$ of the identified dust mass, while corundum takes up (38 ± 3) wt.%. Depending on the choice of continuum, a range of mass fractions is observed for periclase ranging from $(2.7 \pm 1.7)\%$ in the most conservative case to $(9 \pm 2)\%$ in a less constrained continuum. In addition, we identify a feature at $11.2 \mu\text{m}$ as the crystalline silicate forsterite, with only a minor contribution from polycyclic aromatic hydrocarbons. The $(5 \pm 3)\%$ crystalline silicate fraction requires high temperatures such as those found in the immediate quasar environment in order to counteract rapid destruction from cosmic rays.

Subject headings: galaxies: active — quasars: emission lines — quasars: individual (PG 2112+059) — ISM: dust, extinction

¹School of Physics and Astronomy, University of Manchester, Sackville Street, PO Box 88, Manchester, M60 1QD, UK; *F.Markwick-Kemper@manchester.ac.uk*

²University of Virginia, Department of Astronomy, PO Box 400325, Charlottesville, VA 22904-4325, USA

³Department of Physics & Astronomy, University of California – Los Angeles, 430 Portola Plaza, Box 951547, Los Angeles CA, 90095–1547, USA; *sgall@astro.ucla.edu*

⁴Space Sciences Institute, 4750 Walnut Street, Suite 205 Boulder, CO 80301, USA; *dhines@as.arizona.edu*

⁵Max-Planck-Institute for Astronomy, Königstuhl 17, D-69117 Heidelberg, Germany; *bouwman@mpia.de*

1. Introduction

In the local Universe, Asymptotic Giant Branch (AGB) stars are believed to dominate dust production (e.g., Draine 2003). AGB stars are a late phase of stellar evolution for stars with initial masses of $M=1-8M_{\odot}$, which develop outflows where the low temperatures and high densities become optimal for dust condensation. However, a significant amount of dust originating from AGB stars does not build up within ~ 1 Gyr of the birth of the first generation of low-mass stars (Morgan & Edmunds 2003). Nevertheless, large quantities of dust are clearly present at these early times: quasar host galaxies at $z \sim 6$ show evidence for $10^{8-9} M_{\odot}$ of dust heated by star formation in their host galaxies as seen in submm and far-infrared emission (Priddey et al. 2003; Beelen et al. 2006). Furthermore, extinction curves for a $z = 6.2$ quasar and GRB 050904 ($z = 6.29$) are not consistent with those locally (Maiolino et al. 2004; Stratta et al. 2007). Another mechanism for dust production is therefore required, and Elvis et al. (2002) explored the possibility that quasar winds might provide environments suitable for efficient dust formation. They determined that the temperatures and pressures in these regions could reach the values found in cool, dust-producing stars. The quasar winds are predicted to produce dust masses up to $10^7 M_{\odot}$ (Elvis et al. 2002), implying that the quasar wind may in some cases only account for part of the dust production, and supernovae have been suggested as an alternative source of dust in high- z galaxies (Sugerman et al. 2006).

Quasar outflows are most obviously manifested in Broad Absorption Line (BAL) quasars. This population, approximately 20% of optically selected type 1 quasar samples (e.g., Hewett & Foltz 2003; Reichard et al. 2003), is notable for broad, blueshifted absorption evident in common ultraviolet resonance transitions such as C IV, Ly α , and O VI. These P Cygni-type features arise because the observer is looking through an outflowing wind. BAL quasars are thus a natural population to consider when investigating the grain properties of dust in the quasar environment. In this letter, we present a detailed analysis of the mid-infrared spectrum of the luminous BAL quasar, PG 2112+059, in order to determine its dust composition. PG 2112+059, an *IRAS* source, is mid-infrared bright, and one of the most luminous low-redshift ($z = 0.466$) Bright Quasar Survey objects with $M_V = -26.9$ ($H_0 = 70 \text{ km s}^{-1} \text{ Mpc}^{-1}$, $\Omega_M = 0.3$, and $\Omega_{\Lambda} = 0.7$ are assumed throughout). *HST* spectra revealed broad, shallow C IV absorption, and it has been well-studied in the UV and X-ray (e.g., Gallagher et al. 2004).

2. Observations and Data Reduction

PG 2112+059 was observed on May 25, 2005, using the low resolution modules of

the InfraRed Spectrograph (IRS; Houck et al. 2004) on board *Spitzer* (Werner et al. 2004), under AOR key 10949376. We performed 1 cycle of 240 sec. integrations with the short low modules (5.2–14.5 μm) and 2 cycles of 120 sec. with the long low modules (14.0–38.0 μm).

We applied the data reduction, background subtraction and flux calibration methods described in Bouwman et al. (2006); Bouwman et al. (2007); Swain et al. (2007) to pipeline version S14 of the data. The resulting absolute flux is accurate to $\sim 5\%$, while the relative fluxes are accurate to $\sim 1.7\%$. The resulting combined spectrum is shown in Fig. 1.

3. Analysis and Results

The spectrum of PG 2112+059 exhibits the broad emission bands at ~ 10 and ~ 18 μm generally ascribed to amorphous silicates (e.g. Draine 2003). In addition, the [Ne II] transition at 12.8 μm is visible, as well as substructure in the solid state emission at ~ 11.2 μm (Fig. 1).

3.1. Continuum Determination

Complementary to the IRS spectrum, we added mid-IR photometry from the literature as compiled by NED¹ (see Figure 1). In wavelength regions in common, we found good agreement between (all observed-frame wavelengths) 25 μm *IRAS* data (Sanders et al. 1989), 12 and 7.5 μm *ISO* data (Haas et al. 2000), and 10 μm Palomar data (Neugebauer et al. 1987). To determine the continuum underlying the dust emission features, we fit a power-law model ($F_\nu = F_{\nu,0}\nu^\alpha$) using the photometric and spectroscopic data (and uncertainties) from 5–8 μm and 24.5–40 μm (rest-frame). As shown in Figure 1, this provided a good fit to the continuum with $\alpha = -0.617 \pm 0.004$. We note that there is no evidence from quasar composite spectral energy distributions for an inflection under the dust emission features (see Richards et al. 2006), and a power-law model fits the luminous quasar composite in this spectral regime quite well. Because the continuum is not well constrained at wavelengths longer than the broad 18 μm emission feature, we performed a second fit including the 13–14 μm IRS data at the dip between the 10 and 18 μm emission features. This pulled the continuum up to the value of the 60 μm *IRAS* photometric datapoint plus uncertainty for $\alpha = -0.674 \pm 0.003$.

¹NASA/IPAC Extragalactic Database; <http://nedwww.ipac.caltech.edu>

3.2. Spectral Feature Analysis

Assuming the emission region is optically thin in the infrared, the continuum-divided spectrum (Fig. 2) yields the resulting opacity of the dust. As at each wavelength, features and continuum contributions are in equal amounts arising from the same temperature components (e.g. Siebenmorgen et al. 2005), the temperature dependence has been eliminated by dividing the spectra by the continua. The contribution of synchrotron emission to the continuum at these wavelengths can be ignored (Haas et al. 1998).

We fitted the resulting opacity curves with laboratory spectroscopy of minerals commonly observed in AGB stars, assuming that the resulting opacity is a linear combination of the individual mineral opacities. We also subtracted a spline-fit continuum between our fit boundaries – 8 and 25 μm – of each mineral spectrum, to provide the same baseline. For each continuum divided spectrum, we ran 512 models with varying dust compositions (amorphous and crystalline olivine, Al_2O_3 , MgO , polycyclic aromatic hydrocarbons (PAHs); based on prior observations and model calculations, see e.g. Draine 2003) and grain shape (spherical or non-spherical; Bohren & Huffman 1983), to find the relative mass fractions in each component. The fit was performed using χ^2 minimization of each continuum-divided spectrum, excluding the 12.8 μm [NeII] line.

Fig. 2 shows the best fits for both continuum-divided spectra, with $\Delta\chi^2$ values of 2.8 for continuum 1 and 2.6 for continuum 2. If we allow a tolerance of a factor 2 for $\Delta\chi^2$, we find classes of dust compositions containing 44 and 124 good fits; 30 and 47 of which require the presence of PAHs over the 8–25 μm range, for the first and second continuum respectively.

The essential dust components in this class of fits are amorphous olivine – MgFeSiO_4 (Dorschner et al. 1995) and/or Mg_2SiO_4 (Jäger et al. 2003) crystalline forsterite (Koike et al. 1999), corundum (Al_2O_3 ; Begemann et al. 1997) and periclase (MgO ; Hofmeister et al. 2003). For the 20 μm excess in the spectrum not explained by the silicates, we find that MgO in non-spherical grains (represented by a common distribution of ellipsoids) provides a good match. Both spherical and non-spherical grains give good results for the amorphous olivines and corundum. Including grains with radii $a \gtrsim 1 \mu\text{m}$ greatly increased the $\Delta\chi^2$ of the fits, and are therefore not likely to contribute to the observed emission features. The fit results are summarized in Table 1.

The dust mixture is very similar for both continuum-divided spectra, with the notable exception of the MgO mass fraction. In case of the second continuum, where the 13-14 micron range was included in the continuum fit, the MgO contribution is suppressed, but when the 13-14 micron range is –more realistically– treated as dust feature emission, and is not used to constrain the continuum, we find that ~ 9 wt.% of the dust may be in the form

of MgO.

To measure the contribution of PAHs to the emission, we used an average interstellar profile for the PAHs from Hony et al. (2001). Although they contribute to the 11.2 μm feature, the PAHs do not reproduce its shape well, and additional opacity from forsterite is needed. We find that PAHs are responsible for $\sim 30\%$ and $\sim 15\%$ for the first and second continuum respectively. This is consistent with the appearance of the PG 2112+059 spectrum in the 5–9 μm range (Fig. 2). The 11.2 μm resonance in PAHs is likely due to neutral molecules, while the features in the 5–9 μm range are predominantly carried by ionized PAHs (e.g. van Dienenhoven et al. 2004). A range of a factor ~ 6 in $I_{11.2}/I_{6.2}$ around the interstellar value is observed in Galactic environments covering more than 4 orders of magnitude in G_0 (Hony et al. 2001). In case G_0 is significantly stronger than the prevalent field in the Galaxy, $I_{11.2}/I_{6.2}$ decreases, further limiting the amount of PAHs contributing to the 11.2 μm feature.

4. Dust composition

The presence of silicates in local AGN has been known for many years through resonant absorption at 9.7 and 18 μm (e.g., Imanishi & Ueno 2000), while more recently, silicate features have also been detected in emission towards several quasars and AGN (Siebenmorgen et al. 2005; Sturm et al. 2005; Hao et al. 2005; Shi et al. 2006).

While the spectral appearance of PG 2112+059 in the infrared clearly requires silicates, it is interesting that oxides appear to be present as well. As a source of opacity, corundum and periclase cause the 18 μm feature to become stronger relative to the 9.7 μm resonance, while at the same time, they do fill in the opacity trough between the two silicate resonances (see also Jäger et al. 2003). Corundum also causes a red wing on the 9.7 μm resonance, which fits well with the feature as observed in PG 2112+059. This is the first reported detection of periclase and corundum as dust components in a quasar.

4.1. Corundum

The presence of Al_2O_3 is not surprising; it is commonly found in the stellar winds of AGB stars (e.g. Sloan & Price 1998). In thermodynamic equilibrium, corundum (Al_2O_3) is expected to condense at ~ 1500 K, well above the stability limit for silicates (Tielens 1990). In a cooling gas newly condensed Al_2O_3 grains will gradually be covered by silicate layers as the temperature drops, provided the density of the gas does not decrease too rapidly. In cases where the gas density has become too low for significant dust growth once

the gas temperature has reached the stability limits for silicates, a *freeze-out* of the dust condensation sequence occurs, and Al_2O_3 remains the dominant dust component. Indeed, AGB stars with low mass loss rates ($10^{-9} - 10^{-7} M_\odot \text{ yr}^{-1}$) contain significant fractions of Al_2O_3 (Blommaert et al. 2006; Heras & Hony 2005), and a decrease in Al_2O_3 content is observed with increasing mass loss rate for AGB stars in the LMC (Dijkstra et al. 2005).

Both the luminosity and presence of silicates in emission in PG 2112+059 (rather than absorption; Smith et al. e.g., 2007) argue for geometrically associating these grains with the quasar rather than the host galaxy (Shi et al. 2006). The presence of both corundum and olivines in the spectrum indicate that there is a highly inhomogeneous – clumpy – density structure in the dust forming regions as expected from the broad-band spectral modeling of Nenkova et al. (2002) and the theoretical work of Elitzur & Shlosman (2006). As the gas travels outwards, certain pockets apparently maintain high enough density throughout the cooling process that silicates can be formed on top of the corundum, whereas in lower density regions of the wind the dust condensation sequence gets truncated after the formation of Al_2O_3 .

4.2. Periclase

Periclase (MgO) has its stability limits ~ 50 K below the stability limits of Mg-rich olivines (~ 1100 K), but just above the evaporation temperature of Fe – the temperature below which Fe^{2+} can be incorporated in the amorphous silicates (Gail & Sedlmayr 1999; Ferrarotti & Gail 2003). In the thermodynamic equilibrium of a slowly cooling gas, Mg_2SiO_4 would form first, consuming all available gas-phase Mg in the process, thus prohibiting the formation of MgO (Ferrarotti & Gail 2003). The presence of solid MgO in PG 2112+059 indicates that the dust forming gas cooled rapidly to a temperature below these stability limits, allowing for the formation of MgO and Fe-containing silicates at the same time as the formation of Mg_2SiO_4 .

4.3. Amorphous silicates

The amorphous silicates in PG 2112+059 have the stoichiometry of a Mg-rich olivine. By using both Mg_2SiO_4 and MgFeSiO_4 to fit the spectrum, we have determined that the Fe-content of the amorphous silicates is low: $\text{Mg}_{1.95}\text{Fe}_{0.05}\text{SiO}_4$, although using only Mg_2SiO_4 or MgFeSiO_4 gives good results, too. The silicate grains are found to be sub-micron-sized (at $10 \mu\text{m}$ the opacity of silicates is the same for all grain sizes $\lesssim 0.5 \mu\text{m}$), but the data did

not allow us to distinguish between spherical or non-spherical grains. These results compare well to the silicates in the Galactic interstellar medium, which are composed of spherical olivine grains (Kemper et al. 2004), or even more general, of non-spherical Mg-rich olivines (Min et al. 2007).

Attempts to determine the silicate properties in active galaxies include a fit to the 9.7 μm absorption feature seen in NGC 1068, which shows evidence for the presence of Al-bearing species, either in the form of aluminum-silicates or corundum, giving rise to a red wing to the silicate resonance (Jaffe et al. 2004), while Sturm et al. (2005) notice that the 9.7 and 18 μm emission features seen in NGC 3998 have a different spectral appearance than the silicates in the Galactic ISM. In particular, the 18 μm feature is very strong with respect to the 9.7 μm feature, and the peak positions of the resonances deviate as well. We suggest that in NGC 3998, as well as in some quasars (Shi et al. 2006), the broad ‘silicate’ features might be more accurately modeled with a mixture of silicates, corundum and MgO, not unlike PG 2112+059.

4.4. Crystalline silicates

A fraction of $(5\pm3)\%$ by weight of the silicates is found to be crystalline. Evidence of crystalline silicates is not reported in any other silicate emission spectra seen in quasars or AGN, though a feature seen at 11.2 μm in some objects is identified with PAHs, supported by the detection of additional PAH resonances at 6.2 and 7.7 μm (Schweitzer et al. 2006). We only ascribe a small fraction of the emission around 11.2 μm to PAHs (see Sect. 3.2). Crystalline silicates are not detected in the interstellar medium of our own Galaxy (< 2.2 wt.%; Kemper et al. 2005), due to radiation damage caused by cosmic rays on a time scale of 40 Myr. In quasars, the times scales may be even shorter if the cosmic ray flux is higher, and crystalline silicates need to be reformed continuously to explain the observed abundance. The formation of crystalline silicates requires higher densities than amorphous silicates. A quasar wind origin may explain the presence of crystalline silicates in a relatively small fraction (12 out 77) of ultraluminous infrared galaxies (Spoon et al. 2006).

5. Conclusion

For the first time, the composition of the dust in a quasar has been determined, albeit limited to the components with resonances in the infrared. While the origin of the dust could lie in stellar ejecta, the dust properties are consistent with their formation in the quasar

wind itself. The dust in PG 2112+059 clearly bears similarity to dust in other astrophysical environments, i.e. in the properties of the amorphous silicates, but the presence of large amounts of MgO and Al_2O_3 sets it apart from the composition of interstellar dust in the local universe.

Assuming the dust is formed in the quasar wind, the co-existence of the highly refractory corundum, the crystalline silicates and the less refractory MgO and amorphous silicates indicates that the wind of PG 2112+059 has an inhomogeneous temperature and density structure.

This work is based on observations made with the Spitzer Space Telescope, which is operated by the Jet Propulsion Laboratory, California Institute of Technology under a contract with NASA. Support for this work was provided by NASA through an award issued by JPL/Caltech.

Spitzer(IRS)

REFERENCES

- Beelen, A., Cox, P., Benford, D. J., Dowell, C. D., Kovács, A., Bertoldi, F., Omont, A., & Carilli, C. L. 2006, *ApJ*, 642, 694
- Begemann, B., Dorschner, J., Henning, T., Mutschke, H., Gürtler, J., Kömpe, C., & Nass, R. 1997, *ApJ*, 476, 199
- Blommaert, J. A. D. L., et al. 2006, *A&A*, 460, 555
- Bohren, C. F. & Huffman, D. R. 1983, *Absorption and scattering of light by small particles* (New York: Wiley)
- Bouwman, J., Lawson, W. A., Dominik, C., Feigelson, E. D., Henning, T., Tielens, A. G. G. M., & Waters, L. B. F. M. 2006, *ApJ*, 653, L57
- Bouwman, J., et al. 2007, *ApJ*, submitted
- Dijkstra, C., Speck, A. K., Reid, R. B., & Abraham, P. 2005, *ApJ*, 633, L133
- Dorschner, J., Begemann, B., Henning, T., Jäger, C., & Mutschke, H. 1995, *A&A*, 300, 503
- Draine, B. T. 2003, *ARA&A*, 41, 241

- Elitzur, M. & Shlosman, I. 2006, *ApJ*, 648, L101
- Elvis, M., Marengo, M., & Karovska, M. 2002, *ApJ*, 567, L107
- Ferrarotti, A. S. & Gail, H. P. 2003, *A&A*, 398, 1029
- Gail, H.-P. & Sedlmayr, E. 1999, *A&A*, 347, 594
- Gallagher, S. C., Brandt, W. N., Wills, B. J., Charlton, J. C., Chartas, G., & Laor, A. 2004, *ApJ*, 603, 425
- Haas, M., Chini, R., Meisenheimer, K., Stickel, M., Lemke, D., Klaas, U., & Kreysa, E. 1998, *ApJ*, 503, L109
- Haas, M., Müller, S. A. H., Chini, R., Meisenheimer, K., Klaas, U., Lemke, D., Kreysa, E., & Camenzind, M. 2000, *A&A*, 354, 453
- Hao, L., et al. 2005, *ApJ*, 625, L75
- Heras, A. M. & Hony, S. 2005, *A&A*, 439, 171
- Hewett, P. C. & Foltz, C. B. 2003, *AJ*, 125, 1784
- Hofmeister, A. M., Keppel, E., & Speck, A. K. 2003, *MNRAS*, 345, 16
- Hony, S., Van Kerckhoven, C., Peeters, E., Tielens, A. G. G. M., Hudgins, D. M., & Allamandola, L. J. 2001, *A&A*, 370, 1030
- Houck, J. R., et al. 2004, *ApJS*, 154, 18
- Imanishi, M. & Ueno, S. 2000, *ApJ*, 535, 626
- Jaffe, W., et al. 2004, *Nature*, 429, 47
- Jäger, C., Dorschner, J., Mutschke, H., Posch, T., & Henning, T. 2003, *A&A*, 408, 193
- Kemper, F., Vriend, W. J., & Tielens, A. G. G. M. 2004, *ApJ*, 609, 826
- 2005, *ApJ*, 633, 534
- Koike, C., Tsuchiyama, A., & Suto, H. 1999, in *Proc. 32nd ISAS Lunar Planet. Symp.*, 175–178
- Maiolino, R., Schneider, R., Oliva, E., Bianchi, S., Ferrara, A., Mannucci, F., Pedani, M., & Roca Sogorb, M. 2004, *Nature*, 431, 533

- Min, M., Waters, L. B. F. M., de Koter, A., Hovenier, J. W., Keller, L. P., & Markwick-Kemper, F. 2007, *A&A*, 462, 667
- Morgan, H. L. & Edmunds, M. G. 2003, *MNRAS*, 343, 427
- Nenkova, M., Ivezić, Ž., & Elitzur, M. 2002, *ApJ*, 570, L9
- Neugebauer, G., Green, R. F., Matthews, K., Schmidt, M., Soifer, B. T., & Bennett, J. 1987, *ApJS*, 63, 615
- Priddey, R. S., Isaak, K. G., McMahon, R. G., Robson, E. I., & Pearson, C. P. 2003, *MNRAS*, 344, L74
- Reichard, T. A., et al. 2003, *AJ*, 125, 1711
- Richards, G. T., et al. 2006, *ApJS*, 166, 470
- Sanders, D. B., Phinney, E. S., Neugebauer, G., Soifer, B. T., & Matthews, K. 1989, *ApJ*, 347, 29
- Schweitzer, M., et al. 2006, *ApJ*, 649, 79
- Shi, Y., et al. 2006, *ApJ*, 653, 127
- Siebenmorgen, R., Haas, M., Krügel, E., & Schulz, B. 2005, *A&A*, 436, L5
- Sloan, G. C. & Price, S. D. 1998, *ApJS*, 119, 141
- Smith, J. D. T., et al. 2007, *ApJ*, 656, 770
- Spoon, H. W. W., et al. 2006, *ApJ*, 638, 759
- Stratta, G., Maiolino, R., Fiore, F., & D’Elia, V. 2007, *ApJ*, 661, L9
- Sturm, E., et al. 2005, *ApJ*, 629, L21
- Sugerman, B. E. K., et al. 2006, *Science*, 313, 196
- Swain, M. R., Bouwman, J., Akeson, R., Lawler, S., & Beichman, C. 2007, **astro-ph/0702593**
- Tielens, A. G. G. M. 1990, in *From Miras to Planetary Nebulae: which path for stellar evolution?*, eds. M. O. Mennessier & A. Omont, 186–200
- van Diedenhoven, B., Peeters, E., Van Kerckhoven, C., Hony, S., Hudgins, D. M., Allamandola, L. J., & Tielens, A. G. G. M. 2004, *ApJ*, 611, 928

Werner, M. W., et al. 2004, ApJS, 154, 1

Table 1. Best $\Delta\chi^2$ fits to the two continuum-divided spectra of PG 2112+059 (Fig. 2). The first column shows the dust fraction considered, and the following columns show the mass fractions for both continuum fits and the average. The standard deviation on the results is determined from the spread of the mass fractions observed in those fits within the $\Delta\chi^2$ tolerance of a factor 2. The bottom line shows the average composition of the amorphous silicate dust.

	continuum 1	continuum 2	average
	wt.%	wt.%	wt.%
silicates/total	(54 ± 1)	(59 ± 1)	(56.5 ± 1.4)
corundum/total	(37 ± 2)	(39 ± 2)	(38 ± 3)
MgO/total	(9 ± 2)	(2.7 ± 1.7)	(5.9 ± 2.6)
crystalline/silicates	(4 ± 2)	(6 ± 2)	(5 ± 3)
Mg ₂ SiO ₄ /am. silicates	(70 ± 44)	(49 ± 40)	...
MgFeSiO ₄ /am. silicates	(30 ± 44)	(51 ± 40)	...
am. sil. composition	Mg _{1.9} Fe _{0.1} SiO ₄	Mg _{1.8} Fe _{0.2} SiO ₄	Mg _{1.85} Fe _{0.15} SiO ₄

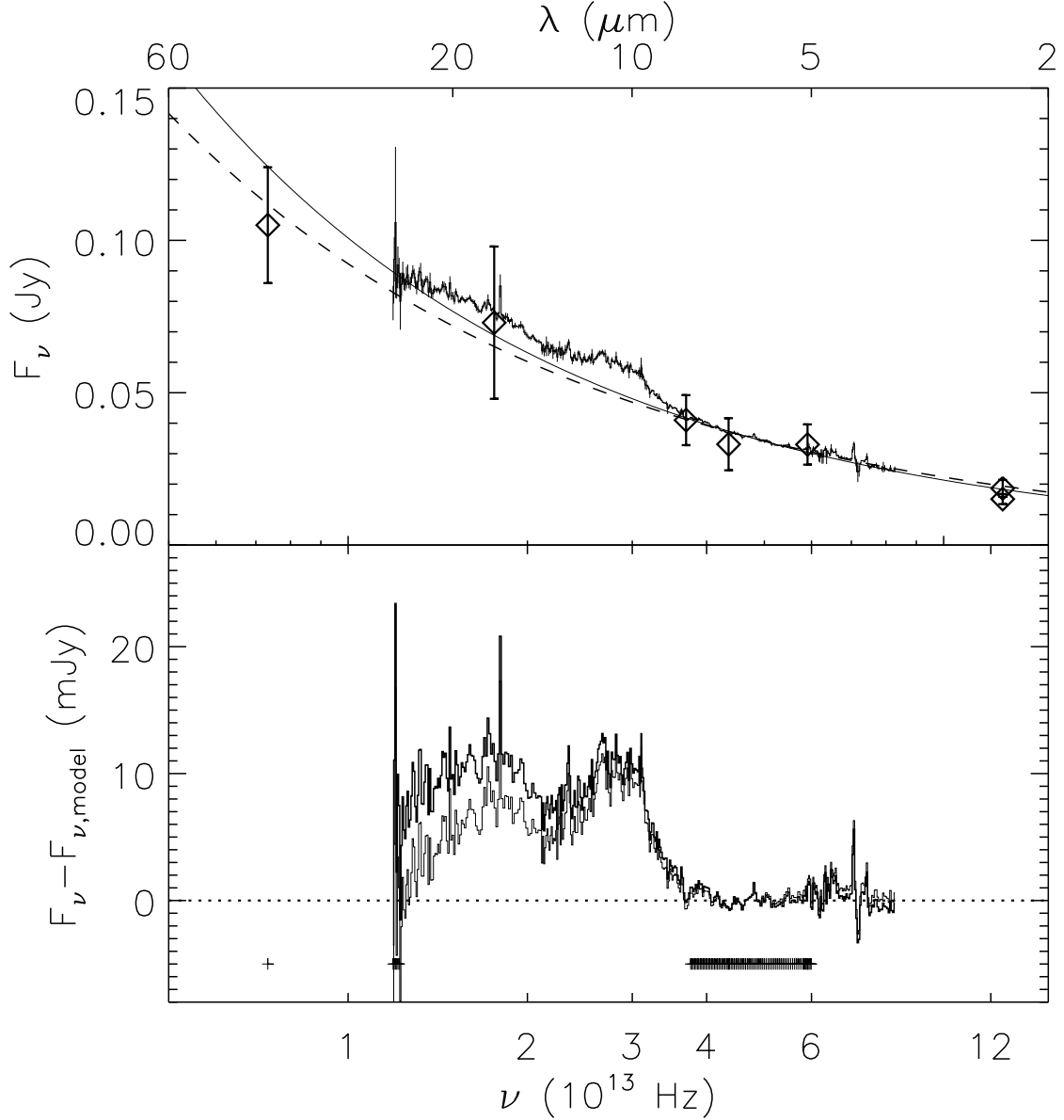


Fig. 1.— (*Top panel*) Mid-infrared spectrum of PG2112+059; the abscissas are rest-frame values. The diamonds are photometric data from the following sources (from left to right, given in observed-frame units): *IRAS* 60 and 25 μm (Sanders et al. 1989), *ISO* 12 μm (Haas et al. 2000), Palomar 10 μm (Neugebauer et al. 1987), *ISO* 7.5 μm (Haas et al. 2000), Palomar 3.5 μm (two observations; Neugebauer et al. 1987). Shown is the IRS spectrum (with error bars), and the dashed and thin solid curves are two power-law continuum models (*Bottom panel*) The IRS spectrum minus the dashed continuum fit (continuum 1; thick solid histogram) and thin solid continuum fit (continuum 2; thin histogram) shown in the top panel. The crosses indicate the frequencies of the data used in the dashed continuum fit; for the second continuum fit, the IRS data from 13–14 μm ($[2.30\text{--}2.14] \times 10^{13}$ Hz) were also included.

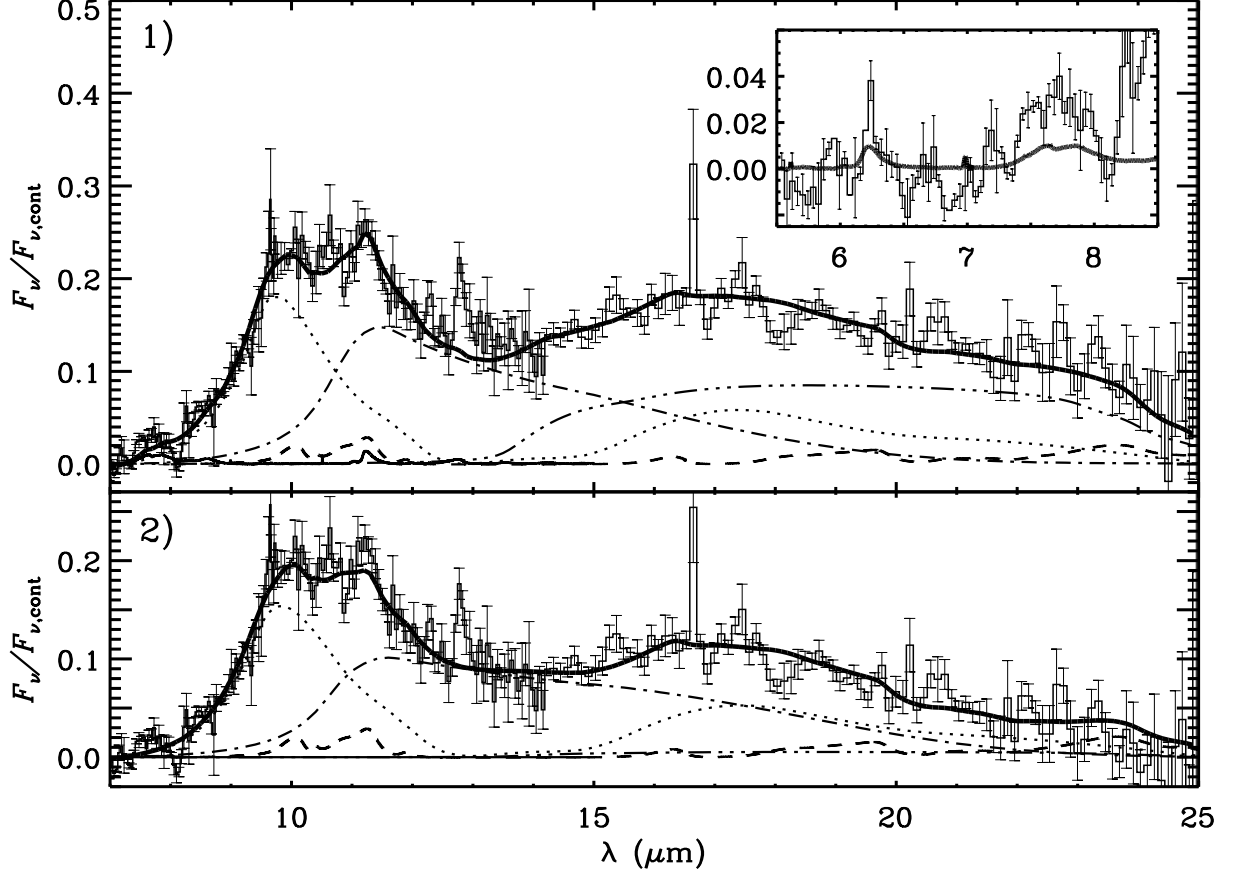


Fig. 2.— Best 8–25 μm fits, from our suite of good fits, for the continuum-divided spectrum of PG 2112+059 (offset by -1) using the first and second choice of continuum (top and bottom panel, respectively). The thick solid line is the total fit to the data (histogram, with error bars) composed of amorphous olivine (dotted line), forsterite (dashed line), corundum (Al_2O_3 , dash-dotted line), MgO (dash-triple-dotted line), and the mean interstellar PAH spectrum (solid line; only in panel 1). The inset in panel 1 shows the strength of PAH features expected in the 5.5–8.5 μm range for a radiation field comparable to that of the Galaxy.